PHYSICAL REVIEW C **75**, 054906 (2007)

Mass, quark-number, and $\sqrt{s_{NN}}$ dependence of the second and fourth flow harmonics in ultrarelativistic nucleus-nucleus collisions

B. I. Abelev,[50] M. M. Aggarwal,[30] Z. Ahammed,[45] B. D. Anderson,[20] D. Arkhipkin,[13] G. S. Averichev,[12] Y. Bai,[28] J. Balewski,[17] O. Barannikova,[9] L. S. Barnby,[2] J. Baudot,[18] S. Baumgart,[50] S. Bekele,[29] V. V. Belaga,[12] A. Bellingeri-Laurikainen,[40] R. Bellwied,[48] F. Benedosso,[28] R. R. Betts,[9] S. Bhardwaj,[35] A. Bhasin,[19] A. K. Bhati,[30] H. Bichsel,[47] J. Bielcik,[50] J. Bielcikova,[50] L. C. Bland,[3] S-L. Blyth,[22] M. Bombara,[2] B. E. Bonner,[36] M. Botje,[28] J. Bouchet,[40] A. V. Brandin,[26] A. Bravar,[3] T. P. Burton,[2] M. Bystersky,[11] R. V. Cadman,[1] X. Z. Cai,[39] H. Caines,[50] M. Calderón de la Barca Sánchez,[6] J. Callner,[9] J. Castillo,[28] O. Catu,[50] D. Cebra,[6] Z. Chajecki,[29] P. Chaloupka,[11] S. Chattopadhyay,[45] H. F. Chen,[38] J. H. Chen,[39] J. Cheng,[43] M. Cherney,[10] A. Chikanian,[50] W. Christie,[3] S. U. Chung,[3] J. P. Coffin,[18] T. M. Cormier,[48] M. R. Cosentino,[37] J. G. Cramer,[47] H. J. Crawford,[5] D. Das,[45] S. Das,[45] S. Dash,[15] M. Daugherity,[42] M. M. de Moura,[37] T. G. Dedovich,[12] M. DePhillips,[3] A. A. Derevschikov,[32] L. Didenko,[3] T. Dietel,[14] P. Djawotho,[17] S. M. Dogra,[19] X. Dong,[38] J. L. Drachenberg,[41] J. E. Draper,[6] F. Du,[50] V. B. Dunin,[12] J. C. Dunlop,[3] M. R. Dutta Mazumdar,[45] V. Eckardt,[24] W. R. Edwards,[22] L. G. Efimov,[12] V. Emelianov,[26] J. Engelage,[5] G. Eppley,[36] B. Erazmus,[40] M. Estienne,[18] P. Fachini,[3] R. Fatemi,[23] J. Fedorisin,[12] K. Filimonov,[22] P. Filip,[13] E. Finch,[50] V. Fine,[3] Y. Fisyak,[3] J. Fu,[49] C. A. Gagliardi,[41] L. Gaillard,[2] M. S. Ganti,[45] E. Garcia-Solis,[9] V. Ghazikhanian,[7] P. Ghosh,[45] Y. G. Gorbunov,[10] H. Gos,[46] O. Grebenyuk,[28] D. Grosnick,[44] S. M. Guertin,[7] K. S. F. F. Guimaraes,[37] N. Gupta,[19] B. Haag,[6] T. J. Hallman,[3] A. Hamed,[41] J. W. Harris,[50] W. He,[17] M. Heinz,[50] T. W. Henry,[41] S. Hepplemann,[31] B. Hippolyte,[18] A. Hirsch,[33] E. Hjort,[22] A. M. Hoffman,[23] G. W. Hoffmann,[42] D. Hofman,[9] R. Hollis,[9] M. J. Horner,[22] H. Z. Huang,[7] S. L. Huang,[38] E. W. Hughes,[4] T. J. Humanic,[29] G. Igo,[7] A. Iordanova,[9] P. Jacobs,[22] W. W. Jacobs,[17] P. Jakl,[11] F. Jia,[21] P. G. Jones,[2] E. G. Judd,[5] S. Kabana,[40] K. Kang,[43] J. Kapitan,[11] M. Kaplan,[8] D. Keane,[20] A. Kechechyan,[12] D. Kettler,[47] V. Yu. Khodyrev,[32] B. C. Kim,[34] J. Kiryluk,[22] A. Kisiel,[46] E. M. Kislov,[12] S. R. Klein,[42] A. G. Knospe,[50] A. Kocoloski,[23] D. D. Koetke,[44] T. Kollegger,[14] M. Kopytine,[20] L. Kotchenda,[26] V. Kouchpil,[11] K. L. Kowalik,[22] P. Kravtsov,[26] V. I. Kravtsov,[32] K. Krueger,[1] C. Kuhn,[18] A. I. Kulikov,[12] A. Kumar,[30] P. Kurnadi,[7] A. A. Kuznetsov,[12] M. A. C. Lamont,[50] J. M. Landgraf,[3] S. Lange,[14] S. LaPointe,[48] F. Laue,[3] J. Lauret,[3] A. Lebedev,[3] R. Lednicky,[13] C-H. Lee,[34] S. Lehocka,[12] M. J. LeVine,[3] C. Li,[38] Q. Li,[48] Y. Li,[43] G. Lin,[50] X. Lin,[49] S. J. Lindenbaum,[27] M. A. Lisa,[29] F. Liu,[49] H. Liu,[38] J. Liu,[36] L. Liu,[49] Z. Liu,[49] T. Ljubicic,[3] W. J. Llope,[36] H. Long,[7] R. S. Longacre,[3] W. A. Love,[3] Y. Lu,[49] T. Ludlam,[3] D. Lynn,[3] G. L. Ma,[39] J. G. Ma,[7] Y. G. Ma,[39] D. Magestro,[29] D. P. Mahapatra,[15] R. Majka,[50] L. K. Mangotra,[19] R. Manweiler,[44] S. Margetis,[20] C. Markert,[42] L. Martin,[40] H. S. Matis,[22] Yu. A. Matulenko,[32] C. J. McClain,[1] T. S. McShane,[10] Yu. Melnick,[32] A. Meschanin,[32] J. Millane,[23] M. L. Miller,[23] N. G. Minaev,[32] S. Mioduszewski,[41] C. Mironov,[20] A. Mischke,[28] D. K. Mishra,[15] J. Mitchell,[36] B. Mohanty,[22] L. Molnar,[33] C. F. Moore,[42] D. A. Morozov,[32] M. G. Munhoz,[37] B. K. Nandi,[16] C. Nattrass,[50] T. K. Nayak,[45] J. M. Nelson,[2] C. Nepali,[20] P. K. Netrakanti,[33] L. V. Nogach,[32] S. B. Nurushev,[32] G. Odyniec,[22] A. Ogawa,[3] V. Okorokov,[26] M. Oldenburg,[22] D. Olson,[22] M. Pachr,[11] S. K. Pal,[45] Y. Panebratsev,[12] A. I. Pavlinov,[48] T. Pawlak,[46] T. Peitzmann,[28] V. Perevoztchikov,[3] C. Perkins,[5] W. Peryt,[46] S. C. Phatak,[15] M. Planinic,[51] J. Pluta,[46] N. Poljak,[51] N. Porile,[33] J. Porter,[47] A. M. Poskanzer,[22] M. Potekhin,[3] E. Potrebenikova,[12] B. V. K. S. Potukuchi,[19] D. Prindle,[47] C. Pruneau,[48] J. Putschke,[22] I. A. Qattan,[17] G. Rakness,[31] R. Raniwala,[35] S. Raniwala,[35] R. L. Ray,[42] S. V. Razin,[12] J. Reinnarth,[40] D. Relyea,[4] A. Ridiger,[26] H. G. Ritter,[22] J. B. Roberts,[36] O. V. Rogachevskiy,[12] J. L. Romero,[6] A. Rose,[22] C. Roy,[40] L. Ruan,[22] M. J. Russcher,[28] R. Sahoo,[15] T. Sakuma,[23] S. Salur,[50] J. Sandweiss,[50] M. Sarsour,[41] P. S. Sazhin,[12] J. Schambach,[42] R. P. Scharenberg,[33] N. Schmitz,[24] K. Schweda,[22] J. Seger,[10] I. Selyuzhenkov,[48] P. Seyboth,[24] A. Shabetai,[18] E. Shahaliev,[12] M. Shao,[38] M. Sharma,[30] W. Q. Shen,[39] S. S. Shimanskiy,[12] E. P. Sichtermann,[22] F. Simon,[23] R. N. Singaraju,[45] N. Smirnov,[50] R. Snellings,[28] P. Sorensen,[3] J. Sowinski,[17] J. Speltz,[18] H. M. Spinka,[1] B. Srivastava,[33] A. Stadnik,[12] T. D. S. Stanislaus,[44] D. Staszak,[7] R. Stock,[14] A. Stolpovsky,[48] M. Strikhanov,[26] B. Stringfellow,[33] A. A. P. Suaide,[37] M. C. Suarez,[9] N. L. Subba,[20] E. Sugarbaker,[29] M. Sumbera,[11] Z. Sun,[21] B. Surrow,[23] M. Swanger,[10] T. J. M. Symons,[22] A. Szanto de Toledo,[37] J. Takahashi,[37] A. H. Tang,[3] T. Tarnowsky,[33] J. H. Thomas,[22] A. R. Timmins,[2] S. Timoshenko,[26] M. Tokarev,[12] T. A. Trainor,[47] S. Trentalange,[7] R. E. Tribble,[41] O. D. Tsai,[7] J. Ulery,[33] T. Ullrich,[3] D. G. Underwood,[1] G. Van Buren,[3] N. van der Kolk,[28] M. van Leeuwen,[22] A. M. Vander Molen,[25] R. Varma,[16] I. M. Vasilevski,[13] A. N. Vasiliev,[32] R. Vernet,[18] S. E. Vigdor,[17] Y. P. Viyogi,[15] S. Vokal,[12] S. A. Voloshin,[48] W. T. Waggoner,[10] F. Wang,[33] G. Wang,[7] J. S. Wang,[21] X. L. Wang,[38] Y. Wang,[43] J. W. Watson,[20] J. C. Webb,[44] G. D. Westfall,[25] A. Wetzler,[22] C. Whitten, Jr.,[7] H. Wieman,[22] S. W. Wissink,[17] R. Witt,[50] J. Wu,[38] N. Xu,[22] Q. H. Xu,[22] Z. Xu,[3] P. Yepes,[36] I-K. Yoo,[34] V. I. Yurevich,[12] W. Zhan,[21] H. Zhang,[3] W. M. Zhang,[20] Y. Zhang,[38] Z. P. Zhang,[38] Y. Zhao,[38] C. Zhong,[39] J. Zhou,[36] R. Zoulkarneev,[13] Y. Zoulkarneeva,[13] A. N. Zubarev,[12] and J. X. Zuo[39]

(STAR Collaboration)

[1]*Argonne National Laboratory, Argonne, Illinois 60439, USA*

[2]*University of Birmingham, Birmingham, United Kingdom*

[3]*Brookhaven National Laboratory, Upton, New York 11973, USA*

[4]*California Institute of Technology, Pasadena, California 91125, USA*

[5]*University of California, Berkeley, California 94720, USA*

[6]*University of California, Davis, California 95616, USA*

[7]*University of California, Los Angeles, California 90095, USA*

[8]*Carnegie Mellon University, Pittsburgh, Pennsylvania 15213, USA*
[9]*University of Illinois, Chicago, USA*
[10]*Creighton University, Omaha, Nebraska 68178, USA*
[11]*Nuclear Physics Institute AS CR, 250 68 Řež/Prague, Czech Republic*
[12]*Laboratory for High Energy (JINR), Dubna, Russia*
[13]*Particle Physics Laboratory (JINR), Dubna, Russia*
[14]*University of Frankfurt, Frankfurt, Germany*
[15]*Institute of Physics, Bhubaneswar 751005, India*
[16]*Indian Institute of Technology, Mumbai, India*
[17]*Indiana University, Bloomington, Indiana 47408, USA*
[18]*Institut de Recherches Subatomiques, Strasbourg, France*
[19]*University of Jammu, Jammu 180001, India*
[20]*Kent State University, Kent, Ohio 44242, USA*
[21]*Institute of Modern Physics, Lanzhou, People's Republic of China*
[22]*Lawrence Berkeley National Laboratory, Berkeley, California 94720, USA*
[23]*Massachusetts Institute of Technology, Cambridge, Massachusetts 02139-4307, USA*
[24]*Max-Planck-Institut für Physik, Munich, Germany*
[25]*Michigan State University, East Lansing, Michigan 48824, USA*
[26]*Moscow Engineering Physics Institute, Moscow Russia*
[27]*City College of New York, New York City, New York 10031, USA*
[28]*NIKHEF and Utrecht University, Amsterdam, The Netherlands*
[29]*Ohio State University, Columbus, Ohio 43210, USA*
[30]*Panjab University, Chandigarh 160014, India*
[31]*Pennsylvania State University, University Park, Pennsylvania 16802, USA*
[32]*Institute of High Energy Physics, Protvino, Russia*
[33]*Purdue University, West Lafayette, Indiana 47907, USA*
[34]*Pusan National University, Pusan, Republic of Korea*
[35]*University of Rajasthan, Jaipur 302004, India*
[36]*Rice University, Houston, Texas 77251, USA*
[37]*Universidade de Sao Paulo, Sao Paulo, Brazil*
[38]*University of Science & Technology of China, Hefei 230026, People's Republic of China*
[39]*Shanghai Institute of Applied Physics, Shanghai 201800, People's Republic of China*
[40]*SUBATECH, Nantes, France*
[41]*Texas A&M University, College Station, Texas 77843, USA*
[42]*University of Texas, Austin, Texas 78712, USA*
[43]*Tsinghua University, Beijing 100084, People's Republic of China*
[44]*Valparaiso University, Valparaiso, Indiana 46383, USA*
[45]*Variable Energy Cyclotron Centre, Kolkata 700064, India*
[46]*Warsaw University of Technology, Warsaw, Poland*
[47]*University of Washington, Seattle, Washington 98195, USA*
[48]*Wayne State University, Detroit, Michigan 48201, USA*
[49]*Institute of Particle Physics, CCNU (HZNU), Wuhan 430079, People's Republic of China*
[50]*Yale University, New Haven, Connecticut 06520, USA*
[51]*University of Zagreb, Zagreb, HR-10002, Croatia*

(Received 6 January 2007; published 10 May 2007)

We present STAR measurements of the azimuthal anisotropy parameter v_2 for pions, kaons, protons, Λ, $\overline{\Lambda}$, $\Xi + \overline{\Xi}$, and $\Omega + \overline{\Omega}$, along with v_4 for pions, kaons, protons, and $\Lambda + \overline{\Lambda}$ at midrapidity for Au+Au collisions at $\sqrt{s_{NN}} = 62.4$ and 200 GeV. The $v_2(p_T)$ values for all hadron species at 62.4 GeV are similar to those observed in 130 and 200 GeV collisions. For observed kinematic ranges, v_2 values at 62.4, 130, and 200 GeV are as little as 10–15% larger than those in Pb+Pb collisions at $\sqrt{s_{NN}} = 17.3$ GeV. At intermediate transverse momentum (p_T from 1.5–5 GeV/c), the 62.4 GeV $v_2(p_T)$ and $v_4(p_T)$ values are consistent with the quark-number scaling first observed at 200 GeV. A four-particle cumulant analysis is used to assess the nonflow contributions to pions and protons and some indications are found for a smaller nonflow contribution to protons than pions. Baryon v_2 is larger than antibaryon v_2 at 62.4 and 200 GeV, perhaps indicating either that the initial spatial net-baryon distribution is anisotropic, that the mechanism leading to transport of baryon number from beam- to midrapidity enhances v_2 or that antibaryon and baryon annihilation is larger in the in-plane direction.

DOI: 10.1103/PhysRevC.75.054906 PACS number(s): 25.75.Nq, 25.75.Ld

I. INTRODUCTION

In noncentral heavy-ion collisions, the overlapping area has a long axis and a short axis. Rescattering among the system's constituents converts the initial coordinate-space anisotropy to a momentum-space anisotropy [1–3]. The *spatial* anisotropy decreases as the evolution progresses so that the *momentum* anisotropy is most sensitive to the early phase of the evolution—before the spatial asymmetry is washed out [4].

Ultrarelativistic Au+Au collisions at Brookhaven National Laboratory's Relativistic Heavy Ion Collider (RHIC) [5] are studied in part to deduce whether quarks and gluons become deconfined during the early, high-energy-density phase of these collisions. Because the azimuthal momentum-space anisotropy of particle production is sensitive to the early phase of the collision's evolution, observables measuring this anisotropy are especially interesting. The azimuth angle (ϕ) dependence of particle momentum distributions can be expressed in the form of a Fourier series: $dN/d\phi \propto 1 + \sum_n 2v_n \cos n(\phi - \Psi_{\rm RP})$, where $\Psi_{\rm RP}$ is the reaction-plane angle [6,7]. The Fourier coefficients v_n can be measured and used to characterize the azimuthal anisotropy of particle production.

Measurements at two higher RHIC energies ($\sqrt{s_{NN}} = 130$ and 200 GeV) established that charged hadron v_2 rises with p_T for $p_T < 2$ GeV/c and then saturates [8,9]. As predicted by the hydrodynamic calculations [10,11]—where local thermal equilibrium is assumed—v_2 at low p_T ($p_T <$ 1 GeV/c) shows a characteristic dependence on particle mass [12,13]. The v_2 values at $\sqrt{s_{NN}} = 130$ and 200 GeV are as large as those predicted by hydrodynamic calculations. The v_2 values measured at $\sqrt{s_{NN}} = 17.3$ GeV [14], the top energy of the Super Proton Synchrotron (SPS) at CERN, however, are below the hydrodynamic models predictions. In this article, we compare v_2 at $\sqrt{s_{NN}} = 17.3$ and 200 GeV to new measurements at $\sqrt{s_{NN}} = 62.4$ GeV that provide a link between the top RHIC energy and the top SPS energy.

In 200-GeV collisions, kaon, proton, $\Lambda + \overline{\Lambda}$, and $\Xi + \overline{\Xi}$ $v_2(p_T)$ at intermediate p_T depends on the number n_q of constituent quarks in the corresponding hadron [15]. A scaling law—motivated by constituent-quark coalescence or recombination models—can account for the observed splitting between baryons and mesons for v_2 in this intermediate region [15,16]. Within these models, hadron v_2 (v_2^h) is related to the v_2 of quarks (v_2^q) in a quark-gluon phase by the relationship: $v_2^h(p_T^h) \approx n_q v_2^q(n_q p_T^q)$ [17]. Intermediate p_T baryon yields also increase with collision centrality more rapidly than meson yields [15,18]: a behavior also expected from coalescence or recombination models [17]. These models suggest that the large v_2 values at intermediate p_T are developed during a prehadronic phase—a conclusion supported by the recent discovery that multistrange baryons, thought to have smaller hadronic cross sections [19,20], attain v_2 values apparently as large as protons or hyperons [21]. Measurements of v_2 for identified particles may, therefore, help reveal whether v_2 is developed in a deconfined quark-gluon phase and can test whether these possible conclusions may still be valid at lower $\sqrt{s_{NN}}$.

This article is organized as follows: in Sec. II we briefly describe the STAR detector. The analysis procedures are presented in Sec. III. In Sec. IV we present our results. This section includes subsections discussing systematic uncertainties, baryon versus antibaryon v_2, quark-number scaling, the fourth harmonic v_4, and the collision energy dependence of v_2. Our conclusions are then presented in Sec. V.

II. EXPERIMENT

Our data were collected from Au+Au collisions at $\sqrt{s_{NN}} =$ 62.4 and 200 GeV with the STAR detector [22]. STAR's main time projection chamber (TPC) [23] was used for particle tracking and identification with supplementary particle identification provided by time-of-flight (TOF) detectors [24]. We analyzed events from a centrality interval corresponding to 0–80% of the hadronic interaction cross section. As in previous STAR analyses [15], we define the centrality of an event from the number of charged tracks in the TPC having pseudorapidity $|\eta| < 0.5$, $p_T > 0.2$ GeV/c, a distance of closest approach to the primary vertex (DCA) less than 2 cm, and more than 10 measured space points [25]. Only events with primary vertices within 30 cm of the TPC center in the beam direction were analyzed.

STAR's main TPC covers the approximate pseudorapidity region $|\eta| < 1.2$ (for collisions at its center) and 2π in azimuth angle. A 0.5 T magnetic field allows charged particles p_T to be measured above 0.1 GeV/c. At the time of data taking the TOF detectors covered $-1 < \eta < 0$ and $\pi/15$ in azimuth angle. Their timing resolutions are ~110 ps so that pions and kaons can be distinguished for $p_T < 1.8$ GeV/c and protons can be identified up to $p_T = 3.0$ GeV/c.

III. ANALYSIS

We identify particles using three different methods: measurement of specific ionizationenergy-loss per unit length in the TPC gas (dE/dx), TOF measurements, and weak-decay vertex finding. dE/dx measurements for a particle with a given momentum are used for identification at low p_T and in the relativistic-rise region ($p_T > 2.0$ GeV/c), where dE/dx increases logarithmically with $\beta\gamma$ (see Ref. [26] and Fig. 26 in Ref. [27]). The pion sample in the relativistic-rise region is selected based on the deviation between the measured dE/dx of each track and the expected dE/dx for a pion in units of Gaussian standard deviations ($n\sigma_\pi$). For p_T > 2.0 GeV/c, pions are selected with $n\sigma_\pi > 0$ (the top half of the distribution). In this case the purity is estimated to be 98%.

The v_2 of protons is measured in this region by fitting the dE/dx distribution with peaks centered at the predicted dE/dx values. From these fits we can derive the relative fractions of pions (f_π), kaons (f_K), and protons (f_p) as a function of dE/dx. We then measure v_2 for all tracks and plot it versus the dE/dx of the track. Once the relative fractions of each particle are known for each value of dE/dx, and v_2 is know as a function of dE/dx, $v_2(dE/dx)$ can be fit with function:

$$v_2(dE/dx) = f_\pi v_{2,\pi} + f_K v_{2,K} + f_p v_{2,p}, \qquad (1)$$

where the v_2 values for each species ($v_{2,\pi}$, $v_{2,K}$, and $v_{2,p}$) are parameters in the fit and f_π, f_K, and f_p, which are extracted from the dE/dx distribution, are part of the fit function. In the relativistic rise region, kaons do not dominate the dE/dx distribution for any value of dE/dx, so their v_2 values are poorly constrained and are not presented here. We estimated the systematic error on the proton v_2 by varying the relative fractions of the different particles within reasonable limits. The relative change in the proton v_2 ($\delta v_2/v_2$) was less than 3%. The shape and width of the peaks are determined from samples of particles identified by other means, e.g., TOF measurements and K^0_S or Λ decay daughters.

The reaction-plane direction is estimated for each event from the azimuthal distribution of charged tracks. We select tracks using criteria similar to those in Ref. [2]. To avoid self-correlations, we subtract the contribution of a given particle from the total reaction-plane vector. For particles identified through their decays, we subtract the contributions of all the decay products. The reaction-plane resolution is estimated using the subevent method [28] and we correct the observed v_2 to account for the dilution caused by imperfect resolution. The resolution depends on the number of tracks used in the calculation and the magnitude of v_2 and therefore depends on centrality. The resolution for $\sqrt{s_{NN}} = 62.4$ GeV collisions is reduced relative to $\sqrt{s_{NN}} = 200$ GeV collisions by ≈30%. Although the resolution depends on the analysis details, for 62.4 GeV Au+Au collisions it typically has value of approximately 0.50, 0.73, and 0.58, respectively, for the centrality intervals 0–10%, 10–40%, and 40–80%.

IV. RESULTS

In Fig. 1 the minimum-bias, midrapidity v_2 values are shown for inclusive charged hadrons, pions, kaons, protons, $\Lambda + \overline{\Lambda}$, $\Xi + \overline{\Xi}$, and $\Omega + \overline{\Omega}$. The gross features of v_2 at $\sqrt{s_{NN}} = 62.4$ GeV are similar to those observed at $\sqrt{s_{NN}} = 200$ GeV [12,15]. For $p_T < 1.5$ GeV/c, a mass hierarchy is observed with v_2 smaller for heavier particles. The p_T and mass dependencies are *qualitatively* (not necessarily quantitatively) consistent with expectations from hydrodynamic calculations that assume the mean-free-path between interactions is zero [10]. For $p_T > 2$ GeV/c, v_2 reaches a maximum, the mass ordering is broken, and v_2 for protons and hyperons tend to be larger than for either pions or kaons. The v_2 values for protons and $\Lambda + \overline{\Lambda}$ above $p_T = 2$ GeV/c are similar. In this region, the multistrange baryons also exhibit v_2 values similar to protons. Although hadrons containing strange quarks are expected to be less sensitive to the hadronic stage, we do not see a statistically significant reduction in the v_2 values of strange baryons compared to protons. Statistical uncertainties, however, still do not exclude the possibility of some strangeness content dependence for v_2. If v_2 or its hadron species dependence is developed through hadronic interactions, v_2 should depend on the cross sections of the interacting hadrons (with hadrons with smaller cross sections developing less anisotropy). The large v_2 values for $\Xi + \overline{\Xi}$ and $\Omega + \overline{\Omega}$ are consistent with v_2 having been developed before hadronization.

The centrality dependence of identified hadron $v_2(p_T)$ for $\sqrt{s_{NN}} = 62.4$ GeV is shown in Fig. 2. Similar p_T and mass

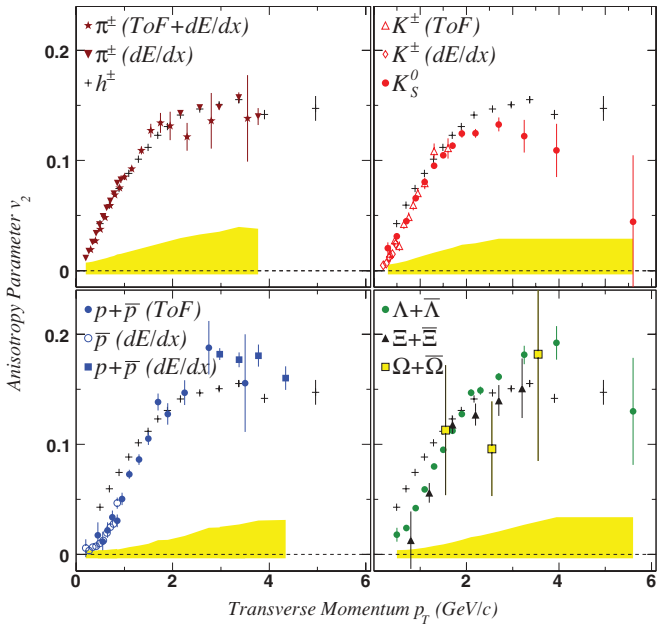

FIG. 1. (Color online) Minimum-bias (0–80% of the collision cross section) $v_2(p_T)$ for identified hadrons at $|\eta| < 1$ from Au+Au collisions at $\sqrt{s_{NN}} = 62.4$ GeV. To facilitate comparisons between panels, v_2 values for inclusive charged hadrons are displayed in each panel. The error bars on the data points represent statistical uncertainties. Systematic uncertainties for the identified particles are shown as shaded bands around $v_2 = 0$.

dependencies are observed for each of the centrality intervals: 0–10%, 10–40%, and 40–80%. The data from the 0–10% interval are most affected by nonflow effects [8], whereas the 10–40% interval is least affected by these uncertainties. The particle-type dependence of nonflow is discussed in the following section.

A. Systematic uncertainties

Systematic uncertainties are shown in Fig. 1 as bands around $v_2 = 0$. The errors are asymmetric. The portions of the band above zero represent the negative errors so that the difference between the measurement and zero is more visually evident. These uncertainties take into account effects from weak-decay feeddown, tracking artifacts, detector artifacts, and nonflow effects. Nonflow effects are dominant. In Fig. 2 the tracking and nonflow systematic uncertainties are shown as bands around $v_2 = 0$ and the weak-decay feeddown uncertainties are included in the error bars on the pion data points.

The number of tracks coming from weak decays that are included in the v_2 analysis depends on the experimental setup and track selection criteria. Pions produced in K^0_S, Λ, or $\overline{\Lambda}$ decays tend to be distributed at low p_T with v_2 values larger than the pions from other sources. We have calculated their effect on the observed pion v_2. We assume exponential m_T spectra for K^0_S and Λ with inverse slope parameters of 285 and 300 MeV, respectively. For relative abundances, we take $K^0_S/(\pi^+ + \pi^-)$ and $(\Lambda + \overline{\Lambda})/(\pi^+ + \pi^-)$ ratios of 0.06 and 0.054, respectively. The v_2 of K^0_S and Λ are taken from data.

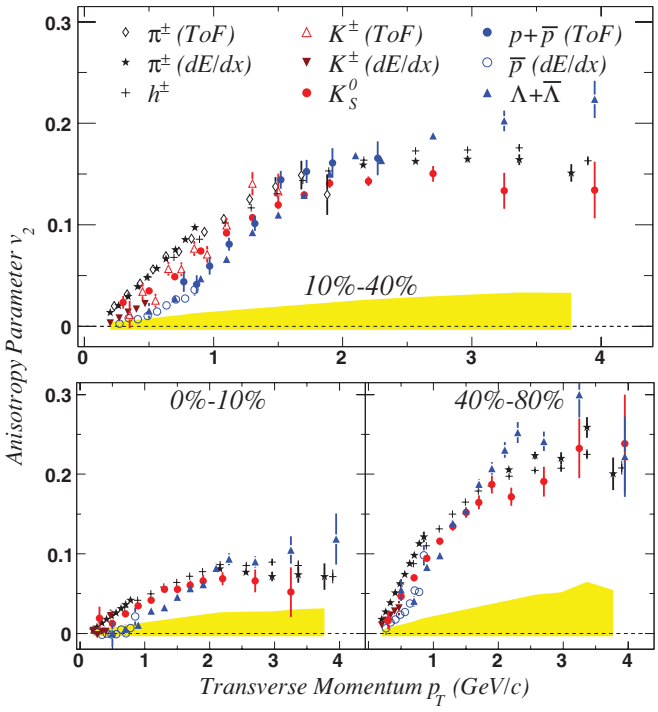

FIG. 2. (Color online) The unidentified charged hadron, charged pion, K^0_S, charged kaon, proton, and $\Lambda + \overline{\Lambda}$ v_2 as a function of p_T for 10–40%, 0–10%, and 40–80% of the Au+Au interaction cross section at $\sqrt{s_{NN}} = 62.4$ GeV. Weak-decay feeddown errors are included in the error bars on the data points, whereas nonflow and tracking error uncertainties are plotted as bands around $v_2 = 0$, which apply to all identified particles. The errors are asymmetric and the portion of the error band above (below) zero represents the negative (positive) error.

We then use a full detector simulation to estimate what fraction of the weak-decay products will fall within our detector acceptance and pass our track selection criteria. We find that for our analysis, feeddown will increase v_2 by approximately 13% (as a fraction of the original v_2) at $p_T = 0.15$ GeV/c. The increase falls to approximately 3% relative at $p_T = 0.25$ GeV/c and is negligible for $p_T > 0.4$ GeV/c. Modifications to the observed proton v_2 from Λ and $\overline{\Lambda}$ decays are neglegible due to the similarity of proton and hyperon v_2.

v_2 measurements can also be distorted by anticorrelations that arise from tracking errors (e.g., track-merging and hit-sharing). These anticorrelations can be eliminated by correlating tracks with $\eta > 0$ ($\eta < 0$) with an event plane determined from tracks at $\eta < -0.15$ ($\eta > 0.15$) (η subevents). This method also has a different sensitivity to the spurious correlations arising from jets and resonance decays (nonflow effects discussed in the next paragraph). In this article, η subevents are used to analyze pion, K^0_S, proton, and $\Lambda + \overline{\Lambda}$ v_2. The remaining systematic uncertainties from detector artifacts are estimated by comparing data taken with different field settings: 0.5 T (full-field) and 0.25 T (half-field). The STAR experiment did not collect half-field data during the 62.4-GeV data-taking period so we use the 200-GeV data to estimate the uncertainties in the 62.4-GeV measurements. From these studies, we assign an uncertainty to v_2 for all particles of ± 0.0035 (absolute).

The dominant systematic uncertainties in v_2 measurements arise from correlations unrelated to the reaction plane (thought to be primarily from correlations between particles coming from jets or resonance decays or other correlations intrinsic to $p + p$ collisions). When v_2 is measured using an event-plane analysis ($v_2\{\text{EP}\}$) [28], these correlations can bias the experimental estimation of the reaction plane (the event-plane angle) and change the apparent v_2 values (nonflow). A four-particle cumulant analysis of v_2 ($v_2\{4\}$) is less sensitive to nonflow effects than a standard analysis but yields larger statistical uncertainties [8]. Although $v_2\{4\}$ has been shown to significantly reduce nonflow uncertainties, some sources of uncertainty may remain: e.g., if v_2 fluctuates from event-to-event $v_2\{4\}$ may yield values smaller than the mean v_2 [29]. The magnitude of possible nonflow correlations for unidentified charged hadrons is discussed in Refs. [8,13]. Here we also discuss variations of nonflow effects between different hadron types.

For $p_T < 1$ GeV/c, a four-particle cumulant analysis is carried out for pions and protons identified with greater than 98% purity. To study the hadron-type dependence of nonflow effects at intermediate p_T, we analyze two samples of charged hadrons at $2.4 < p_T < 3.6$ GeV/c: one with $n\sigma_\pi > 0$, the other with $-5 < n\sigma_\pi < -2.5$. Data from the 10–40% centrality interval are used. For $n\sigma_\pi > 0$, approximately 98% of the charged tracks are pions. For $-5 < n\sigma_\pi < -2.5$, the sample contained approximately 75% protons, 19% kaons, and 6% pions. The ratio of the event-plane v_2 ($v_2\{\text{EP}\}$) to the cumulant v_2 ($v_2\{4\}$) for the pion sample and the proton sample are listed in Table I. In the p_T region below 1 GeV/c, proton v_2 does not appear to manifest any nonflow correlations for either energy. For pions in this region, however, nonflow correlations seem to account for 10% of the v_2 measured with the event-plane analysis.

At intermediate p_T, $v_2\{\text{EP}\}/v_2\{4\}$ is greater than unity for protons and pions. This shows that nonflow correlations increase the observed $v_2\{\text{EP}\}$ for both protons and pions. At 62.4 GeV, the increase is the same (within errors) for both particles. With the larger 200-GeV data set, however, we observe a larger nonflow fraction for pions than protons: the pion $v_2\{\text{EP}\}/v_2\{4\} = 1.22 \pm 0.02$ and $v_2\{\text{EP}\}/v_2\{4\}$ for the proton sample $= 1.16 \pm 0.02$. Pion $v_2\{\text{EP}\}$, therefore, appears to be more susceptible to nonflow correlations than v_2 for particles in the proton sample.

TABLE I. The ratio $v_2\{\text{EP}\}/v_2\{4\}$ (v_2 from a standard event-plane analysis over v_2 from a four-particle cumulant analysis) for the centrality interval 10–40% in three p_T ranges (units for p_T are GeV/c). The sample from $2.4 < p_T < 3.6$ GeV/c labeled as protons contains contamination from pions (6%) and kaons (19%).

p_T	62.4 GeV		200 GeV	
	Pions	Protons	Pions	Protons
0.3–0.5	1.09 ± 0.01	1.01 ± 0.10	1.10 ± 0.01	0.97 ± 0.07
0.5–0.7	1.10 ± 0.01	0.98 ± 0.08	1.09 ± 0.01	0.99 ± 0.05
2.4–3.6	1.08 ± 0.04	1.11 ± 0.05	1.22 ± 0.02	1.16 ± 0.02

B. Baryon vs. antibaryon v_2

To our knowledge, no prediction for a difference between baryon and antibaryon v_2 exists in the literature. Previous measurements at RHIC of identified baryon v_2 reported no differences between Λ and $\overline{\Lambda}$ v_2 or between proton and antiproton v_2. Typically the particle and antiparticle samples were combined. These measurements were made with smaller data samples and at higher energies where the antibaryon-to-baryon yield ratios are much closer to unity. Several scenarios can lead to a difference between antibaryon and baryon v_2 that is larger when the antibaryon-to-baryon yield ratio is smaller: (a) baryons may develop larger momentum-space anisotropies through multiple rescattering as they are transported to midrapidity; (b) if the initial spatial net-baryon density is anisotropic, flow developing in a later stage could convert that spatial anisotropy to an observable momentum-space anisotropy; and (c) annihilation of antibaryons in the medium can reduce the antibaryon yield, with the reduction larger in the more dense, in-plane direction than the out-of-plane direction. We consider scenario (a) and (b) to be distinct. In scenario (a), extra v_2 is built up while the baryons are being transported to midrapidity, whereas in scenario (b) the v_2 is established through rescattering after the baryons are transported to midrapidity.

In Fig. 3 we show the ratio of $\overline{\Lambda}$ v_2 to Λ v_2. The data are from minimum bias Au+Au collisions at 62.4 and 200 GeV. The bands on the figure represent the mean values of the ratios, which are, respectively, 0.948 ± 0.014 and 0.971 ± 0.005 for 62.4 and 200 GeV. In the measured range, the $\overline{\Lambda}$ v_2 is systematically smaller than the Λ v_2 for both energies and within errors is approximately p_T independent (fitting the data with a straight line yields slopes of 0.014 ± 0.028 $(\mathrm{GeV}/c)^{-1}$ and 0.017 ± 0.010 $(\mathrm{GeV}/c)^{-1}$, respectively, for 62.4 and 200 GeV data). The difference between $\overline{\Lambda}$ and Λ v_2 is larger at 62.4 GeV, where the $\overline{\Lambda}/\Lambda$ yield ratio is smaller. Taking into account the $\overline{\Lambda}/\Lambda$ yield ratios (measured to be 0.532 ± 0.014 at 62.4 GeV and 0.77 ± 0.05 at 200 GeV/c [30]), we find that at 62.4 GeV the net Λ v_2 (the asymmetry of the quantity $\Lambda - \overline{\Lambda}$)

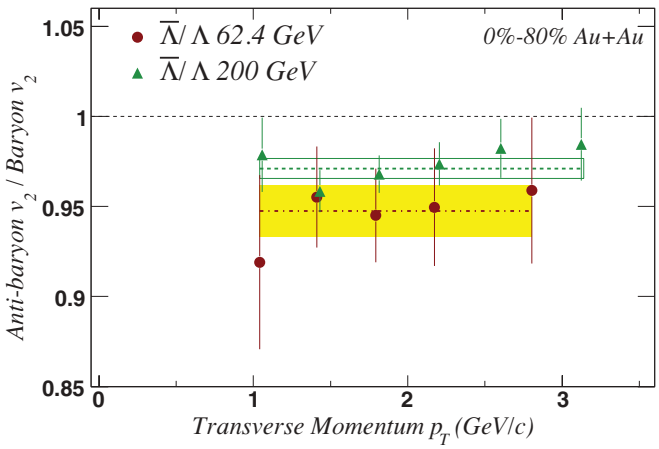

FIG. 3. (Color online) The ratio of $\overline{\Lambda}$ v_2 to Λ v_2. The data are from minimum bias Au+Au collisions at $\sqrt{s_{NN}} = 62.4$ and 200 GeV. The bands show the average values of the ratios within the indicated p_T ranges.

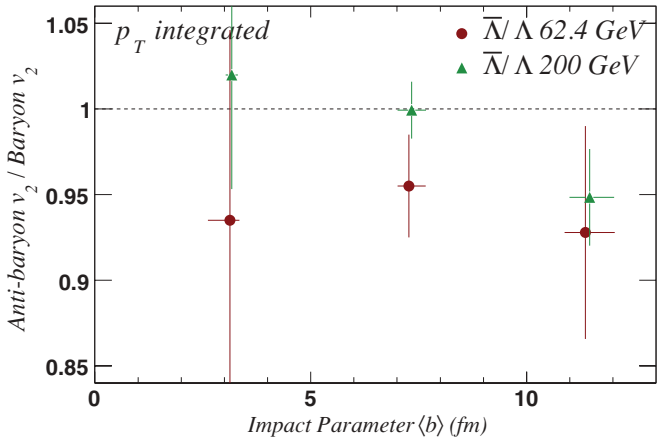

FIG. 4. (Color online) The p_T integrated ratio of $\overline{\Lambda}$ v_2 to Λ v_2 for three centrality intervals: 0–10%, 10–40%, and 40–80%. The data are from Au+Au collisions at $\sqrt{s_{NN}} = 62.4$ and 200 GeV.

is 12% ± 3% larger than the v_2 of all other Λs or $\overline{\Lambda}$s. At 200 GeV it is 13% ± 4% larger. The larger Λ v_2 is not anticipated from the relativistic quantum molecular dynamics (RQMD) hadronic transport model [31] where at midrapidity, the ratio of antiproton v_2 to proton v_2 is 1.148 ± 0.084 and the ratio of $\overline{\Lambda}$ v_2 to Λ v_2 is 1.142 ± 0.123. We note, however, that this model does not reproduce the overall magnitude of v_2 at this energy either.

In Fig. 4 we display the centrality dependence of the p_T integrated $\overline{\Lambda}$ v_2 to Λ v_2 ratio. A Monte Carlo Glauber model is used to convert the centrality intervals defined by multiplicity into mean impact parameter values. Given the errors we are unable to make a definitive statement about a possible dependence of the ratio on centrality.

C. Quark-number scaling

Models of hadron formation by coalescence or recombination of quarks successfully reproduce many features of hadron production in the intermediate p_T region ($1.5 < p_T < 5$ GeV/c) [15–17]. These models find that at intermediate p_T, v_2 may follow a quark-number (n_q) scaling with $v_2(p_T/n_q)/n_q$ for most hadrons falling approximately on one curve. In these models, this universal curve represents the momentum-space anisotropy developed by quarks prior to hadron formation. This scaling behavior was observed in Au+Au collisions at 200 GeV [15]. Approximate quark number scaling of v_2 also exhists in RQMD models where the scaling is related to the additive quark hypothesis for hadronic cross sections [31,32]. The RQMD model, however, underpredicts the value of v_2 by approximately a factor of 2. Prehadronic interactions are therefore thought necessary to generate a v_2 as large as that observed at RHIC. If v_2 is predominantly established in this prehadronic phase, the hadronic cross sections might not play a dominant role in establishing the particle-type dependence of v_2.

Figure 5 shows v_2 scaled by the number of valence quarks in the hadron (n_q) as a function of p_T/n_q (a) and $(m_T - m_0)/n_q$ (b) for identified hadrons at $\sqrt{s_{NN}} = 62.4$ GeV. A polynomial

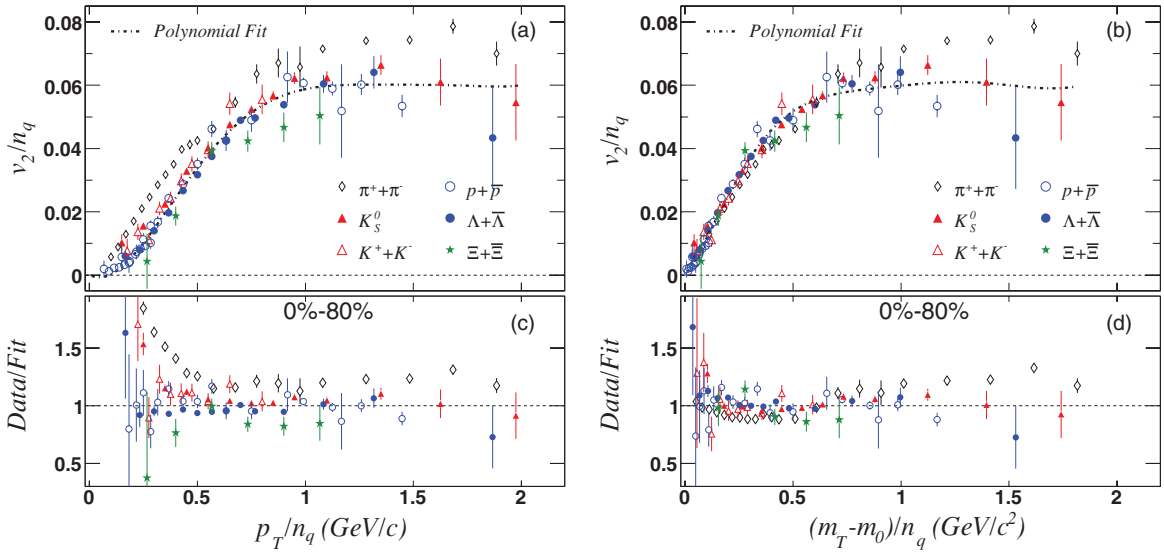

FIG. 5. (Color online) Identified particle v_2 from minimum bias collisions at $\sqrt{s_{NN}} = 62.4$ GeV scaled by the number of valence quarks in the hadron (n_q) and plotted versus p_T/n_q (a) and $(m_T - m_0)/n_q$ (b). In each case a polynomial curve is fit to all particles except pions. The ratio of v_2/n_q to the fit function is shown in the bottom panels (c) and (d).

function has been fit to the scaled values of v_2 for all particles except pions, which, for reasons discussed below, may violate the scaling. To investigate the quality of agreement between hadron species, the data from the top panel are scaled by the fitted polynomial function and plotted in the bottom panels (c) and (d) of Fig. 5. In Fig. 5(c), for $p_T/n_q > 0.6$ GeV/c, the scaled v_2 of K^0_S, $K^{\pm}$, $p + \overline{p}$, and $\Lambda + \overline{\Lambda}$, lie on a single curve, within errors. The 62.4 GeV data for these species are therefore consistent with the scaling observed in 200-GeV collisions. The $\Xi + \overline{\Xi}$ v_2 may lie below the curve but the current errors do not permit a strong conclusion regarding deviations between $\Xi + \overline{\Xi}$ and $p + \overline{p}$ or $\Lambda + \overline{\Lambda}$ v_2. At $p_T/n_q < 0.6$ GeV/c, the scaling breaks down.

It was shown that for 200 GeV at $m_T - m_0 < 0.8$ GeV/c^2, $v_2(m_T - m_0)$ is a linear function and independent of hadron mass [33]. In Figs. 5(b) and 5(d) we combine m_T scaling and n_q scaling so that a single curve can be used to approximately describe v_2 throughout the measured range. This is the same scaling as used in Ref. [34], where the figures are labeled KE_T ($m_T - m_0$ is the transverse kinetic energy). This combined scaling works because in the range where v_2 is a linear function of $m_T - m_0$, dividing by n_q does not alter the shape of the curve. Once it is observed that v_2 for all particles follow the same linear function for $m_T - m_0$, the scaling of $v_2(m_T - m_0)$ with n_q becomes trivial. At higher p_T, v_2 is only weakly dependent on p_T so that changing the axis variable from p_T/n_q to $(m_T - m_0)/n_q$ does not effect the scaling significantly.

Pion v_2 deviates significantly from the fit function in both Figs. 5(a) and 5(b). The contribution of pions from resonance decays to the observed pion v_2 may account for much of the deviation for $p_T < 1.5$ GeV/c [35]. For $p_T > 1.5$ GeV/c, nonflow correlations discussed previously may contribute to the deviation. From the results in Table I, we conclude that nonflow effects tend to be larger for pions than protons. Particularly for the 200 GeV data, removing nonflow contributions will increase the difference between pion and proton v_2 and will improve the agreement between pion v_2/n_q and v_2/n_q for the other measured particles. It has also been suggested that constituent-quark-number scaling may be violated for pions because the pion mass is much smaller than the masses of its constituent quarks. This implies a larger binding energy and a wider wave function for the pion. As a result, the approximation that hadrons coalesce from constituent quarks with nearly collinear momenta is broken [35].

Figure 6 shows v_2/n_q versus $(m_T - m_0)/n_q$ for 0–10%, 10–40%, and 40–80% most central Au+Au collisions at $\sqrt{s_{NN}} = 62.4$ GeV. v_2/n_q for each centrality interval is scaled by the mean eccentricity of the initial overlap region. The eccentricity is calculated from the mean x and y positions of the participating nucleons using a Monte Carlo Glauber model. The coordinate system is shifted and rotated so that (0, 0) is located at the center-of-mass of the participants and the eccentricity is the maximum possible. This is referred to as the participant eccentricity ($\varepsilon_{\text{part}}$). Because the true reaction plane is not known, our v_2 measurements are sensitive to $\varepsilon_{\text{part}}$ [36]. For the 0–10%, 10–40%, and 40–80% centrality intervals the $\langle\varepsilon_{\text{part}}\rangle$ values, respectively, are 0.080, 0.247, and 0.547.

The $m_T - m_0$ and n_q scalings shown for minimum bias data in Fig. 5 are also valid within the specific centrality intervals shown in Fig. 6. Early hydrodynamic calculations predicted that v_2 should approximately scale with the initial spatial eccentricity of the collision system [4]. $v_2/\langle\varepsilon_{\text{part}}\rangle$ contradicts these expectations and rises monotonically as the centrality changes from peripheral to central. This indicates that central collisions are more efficient at converting spatial anisotropy to momentum-space anisotropy.

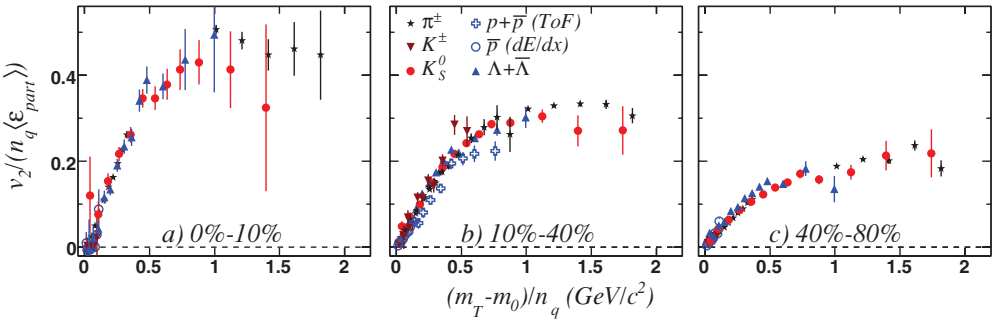

FIG. 6. (Color online) v_2/n_q scaled by the mean eccentricity of the initial overlap region versus $(m_T - m_0)/n_q$ for 0–10%, 10–40%, and 40–80% most central Au+Au collisions at $\sqrt{s_{NN}} = 62.4$ GeV.

D. Fourth harmonic v_4

Higher-order anisotropy parameters (v_4, v_6, etc.) may be sensitive probes of hydrodynamic behavior and the initial conditions of the collision system [37]. The authors of Ref. [38] argue that values of the ratio v_4/v_2^2 larger than 0.5 indicate deviations from ideal fluid behavior. When measured for identified particles, higher harmonics can also test quark-number scaling [39]. v_4 and v_6 for charged hadrons at 200 GeV are shown in Ref. [40]. Identified particle v_4 at 200 GeV is shown in Ref. [13]. In Fig. 7 (top panels) we plot pion, kaon, antiproton, and $\Lambda + \overline{\Lambda}$ v_4 for $\sqrt{s_{NN}} = 62.4$ GeV, where the standard event-plane analysis method has been used. In the bottom panels of Fig. 7 we show the ratio v_4/v_2^2 for charged pions, neutral kaons, and hyperons. The uncertainty in v_4/v_2^2 from possible nonflow leads to asymmetric errors. The ratio v_4/v_2^2 is well above 0.5 even when errors are taken into account.

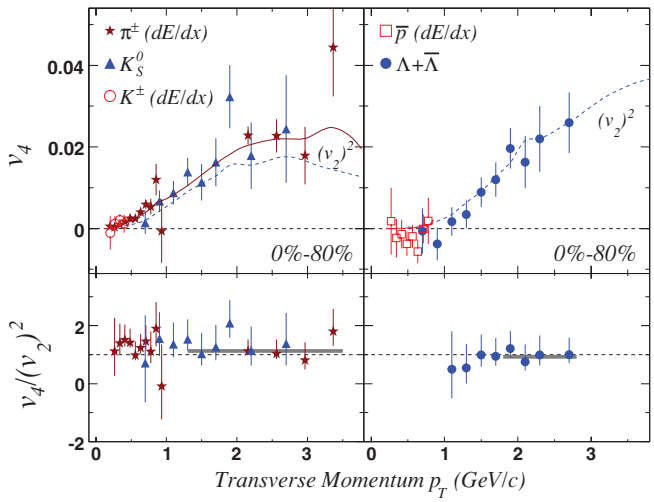

FIG. 7. (Color online) (Top panels) Minimum bias v_4 for pions, charged kaons, K^0_S, antiprotons, and $\Lambda + \overline{\Lambda}$ at $\sqrt{s_{NN}} = 62.4$ GeV. In the left panel the solid (dashed) line shows the value for v_2^2 for pions (kaons). In the right panel the dashed line is v_2^2 for $\Lambda + \overline{\Lambda}$. (Bottom panels) v_4 scaled by v_2^2 (points where v_4 and v_2 fluctuate around zero are not plotted). Gray bands correspond to the fit results described in the text and Table II. The systematic errors on the v_4/v_2^2 ratio from nonflow are included in the error bars leading to asymmetric errors.

In simple coalescence models [39], the ratio v_4/v_2^2 for hadrons is related to v_4/v_2^2 for quarks:

$$\left[v_4/v_2^2\right]^{\text{Meson}}_{2p_T} \approx 1/4 + (1/2)\left[v_4/v_2^2\right]^{\text{Quark}}_{p_T} \tag{2}$$

$$\left[v_4/v_2^2\right]^{\text{Baryon}}_{3p_T} \approx 1/3 + (1/3)\left[v_4/v_2^2\right]^{\text{Quark}}_{p_T}, \tag{3}$$

where here p_T is the quark p_T. The v_4/v_2^2 for mesons can also be related to v_4/v_2^2 for baryons:

$$\left[v_4/v_2^2\right]^{\text{Baryon}}_{3p_T} \approx 1/6 + (2/3)\left[v_4/v_2^2\right]^{\text{Meson}}_{2p_T}. \tag{4}$$

Within this simple model, the large v_4/v_2^2 ratios presented here indicate a large quark v_4. At intermediate p_T, where quark scaling is thought to be valid, we use the equations above to fit v_4/v_2^2 simultaneously for mesons and baryons, with v_4/v_2^2 for quarks as a free parameter. The fit range is $p_T > 1.2$ GeV/c for mesons and $p_T > 1.8$ GeV/c for baryons. A good χ^2 per degree-of-freedom (4.4/13) is found with quark $v_4/v_2^2 = 1.93 \pm 0.29$. The gray bars in the bottom panels of Fig. 7 show the corresponding v_4/v_2^2 values for mesons and baryons. $\langle v_4/v_2^2 \rangle$ values for $p_T/n_q > 0.6$ GeV/c from data and the fit are listed in Table II. Because pion v_2 is known to deviate from the simple scaling laws, we also performed the fit excluding the pion data points (fit II) that yielded a $v_4/v_2^2 = 2.18 \pm 0.40$ and χ^2 per degree-of-freedom of 2.3/9. The small χ^2 values for both fits indicate that our data are consistent with quark-number scaling where quark v_4/v_2^2 is approximately 2.

TABLE II. The ratio v_4/v_2^2 for $p_T/n_q > 0.6$ GeV/c from a combined fit and from data. Pion data points are used for fit I and excluded for fit II. The χ^2 per degree-of-freedom is also shown on the bottom row.

	Data	Fit I	Fit II
$\pi^\pm$	1.10 ± 0.09	1.16 ± 0.16	
K^0_S	1.39 ± 0.19	1.16 ± 0.16	1.33 ± 0.30
$\Lambda + \overline{\Lambda}$	0.98 ± 0.15	0.94 ± 0.10	1.05 ± 0.20
quark		1.93 ± 0.29	2.18 ± 0.40
χ^2/dof		4.4/13	2.3/9

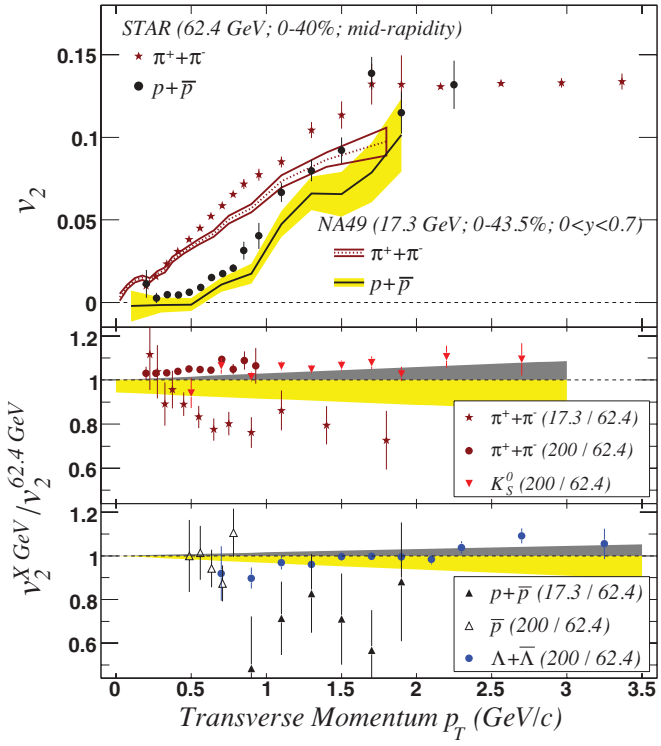

FIG. 8. (Color online) (Top panel) v_2 for pions and protons at $\sqrt{s_{NN}} = 62.4$ and 17.3-GeV. The 62.4-GeV data are from TOF and dE/dx measurements combined. (Middle and bottom panels) Ratios of v_2 for $\pi^+ + \pi^-$, K^0_S, $p + \overline{p}$, $\Lambda + \overline{\Lambda}$ and at different center-of-mass energies scaled by the values at 62.4 GeV. The gray and yellow bands represent systematic uncertainties in the v_2 ratios arising from nonflow effects. The gray bands (above unity) are the uncertainties for the 200-GeV/62.4-GeV data and the yellow bands (below unity) are for the 17.3-GeV/62.4-GeV data.

E. Collision energy dependence

In Fig. 8 (top panel) we plot pion and proton v_2 from $\sqrt{s_{NN}} = 62.4$ Au+Au and 17.3-GeV Pb+Pb collisions [14]. In the bottom panels we show pion, K^0_S, proton, and $\Lambda + \overline{\Lambda}$ data from 17.3 and/or 200 GeV scaled by 62.4-GeV data. The 200 to 62.4 GeV ratios are taken using v_2 data measured within the 0–80% centrality interval. The TOF v_2 measurements presented in this article allow us to show the 17.3 to 62.4 GeV v_2 ratio to higher p_T than the 200-GeV data extends. To approximately match the centrality interval used for the 17.3-GeV data, the 17.3- to 62.4-GeV ratios are taken using, respectively, 0–43.5% and 0–40% centrality intervals. The STAR data at 62.4 and 200 GeV are measured within the pseudorapidity interval $|\eta| < 1.0$ and the 17.3-GeV data are from the rapidity interval $0 < y < 0.7$. These intervals represent similar y/y_{beam} ranges so that measurements at all energies should approximate v_2 at $y = 0$ similarly well. This may be an important constraint because y_{beam} at $\sqrt{s_{NN}} = 17.3$ is only 2.91, whereas NA49 $v_2(p_T)$ results reported in Ref. [14] are from $0 < y < 2.1$. We use the same method to analyze the 200- and 62.4-GeV data.

Systematic errors from weak-decay feeddown and tracking errors will mostly cancel when taking the ratio of v_2 at 200 and 62.4 GeV. Possible nonflow errors are larger at 200 GeV than at 62.4 GeV. In the lower panels of Fig. 8, the shaded bands around unity show the uncertainty in the energy dependence of the v_2 ratio arising from possible changes in the magnitude of nonflow effects at different energies. The portion of the band above unity applies to the ratio of 200- and 62.4-GeV data, whereas the portion below unity only applies to the ratio of the 17.3- and 62.4-GeV data.

The v_2 data for pions and kaons at 62.4 GeV tend to be about 5% smaller than the 200-GeV data (although at $p_T > 1$ GeV/c the difference is within systematic uncertainties). The antiproton data at 62.4 and 200 GeV are consistent within errors. The data exclude a proton v_2 variation between 62.4 and 200 GeV greater than approximately 15%. The $\Lambda + \overline{\Lambda}$ data show a potentially interesting p_T dependence: for $p_T < 1.5$ GeV/c the 200 GeV $\Lambda + \overline{\Lambda}$ v_2 is systematically smaller than the 62.4-GeV data, whereas for $p_T > 1.5$ GeV/c the 200-GeV $\Lambda + \overline{\Lambda}$ v_2 data are consistent with or larger than the 62.4-GeV data. Such a dependence can arise if the system in 200-GeV collisions develops a larger expansion velocity.

Significant differences are seen between the 17.3- and 62.4-GeV data. At $p_T > 0.5$ GeV/c, for both pions and protons, the v_2 values measured at 62.4 GeV are approximately 10–25% larger than those measured at 17.3 GeV [14,41]. Although the magnitude of v_2 is different at the lower energy, the systematics of the particle-type dependencies are similar. In particular, pion v_2 and proton v_2 cross over each other (or attain similar values) at p_T near 1.7 GeV/c for $\sqrt{s_{NN}} =$ 17.3-, 62.4-, and 200-GeV data. Due to the limited kinematic range covered by the 17.3-GeV data, a quark-number dependence of v_2 at intermediate p_T can neither be confirmed nor excluded.

The increase in the magnitude of v_2 from 17.3 to 62.4 GeV and the similarity of 62.4 v_2 to 200 GeV v_2 has been taken as a possible indication for the onset of a limiting behavior [42]. In a collisional picture, a saturation of v_2 could indicate that for $\sqrt{s_{NN}}$ at and above 62.4 GeV the number of collisions the system constituents experience in a given time scale can be considered large and that hydrodynamic equations can therefore be applied. Hydrodynamic model calculations of v_2 depend on the model initialization and the poorly understood freeze-out assumptions [10,11]. As such, rather than comparing the predicted and measured values at one energy, the most convincing way to demonstrate that a hydrodynamic limit has been reached may be to observe the onset of limiting behavior with $\sqrt{s_{NN}}$. For this reason, v_2 measurements at a variety of center-of-mass energies are of interest.

Contrary to the large differences reported by the PHENIX Collaboration in Ref. [42], we find that when the 17.3- and 62.4-GeV $v_2(p_T)$ data for middle rapidity are compared and when possible nonflow systematic uncertainties are accounted for (the yellow bands in the bottom panel of Fig. 8), the differences between $v_2(p_T)$ within the data sets although significant may be as small as 10–15%. A previous comparison of STAR and PHENIX data at $\sqrt{s_{NN}} = 200$ GeV showed that in the p_T range from 0.4 to 0.9 GeV/c, PHENIX measurements of charged pion v_2 are approximately 4–8% higher than equivalent STAR results (see Fig. 11 in Ref. [13]). The $\sqrt{s_{NN}} = 17.3$ GeV charged hadron v_2 data in Ref. [42] is

taken from the CERES Experiment [43]. CERES reports that their measurements of $v_2(p_T)$ are typically 15% smaller than those of NA49. These factors combine to produce a more dramatic energy dependence when comparing PHENIX and CERES data than when comparing STAR and NA49 data. Given the possibly small differences between STAR and NA49 identified particle $v_2(p_T)$, we conclude that a large fraction of the deviation between the SPS data and hydrodynamic models may arise due to the wide rapidity range covered by those measurements (v_2 approaches zero as beam rapidity is approached [44]), increased $\langle p_T \rangle$ values at RHIC and the larger v_2 values predicted for the lower colliding energy by hydrodynamic models.

V. CONCLUSIONS

We presented measurements of v_2 for pions, kaons, protons, Λ, $\overline{\Lambda}$, $\Xi + \overline{\Xi}$, and $\Omega + \overline{\Omega}$ from Au+Au collisions with $\sqrt{s_{NN}} = 62.4$ GeV. We compared these measurements to similar measurements at $\sqrt{s_{NN}} = 17.3$ and 200 GeV. The 62.4-GeV pion, kaon, proton, and hyperon v_2 data are, within a few percentages, consistent with the equivalent data at 200 GeV. Within similar y/y_{beam} intervals and and after we account for systematic uncertainties, we find that for a given identified particle species the difference between 17.3 and 62.4 GeV v_2 data may be as small as 10–15%. We find that Λ v_2 is larger than $\overline{\Lambda}$ v_2 at 62.4 and 200 GeV and that the difference is larger at 62.4-GeV, where the antibaryon to baryon yield ratio is smaller. At both energies our measurements are consistent with net Λ v_2 being approximately 10–15% larger than $\overline{\Lambda}$ and pair-produced Λ v_2.

Our v_2 measurements at 62.4 GeV are consistent with the quark-number scaling of v_2 first observed from Au+Au collisions at $\sqrt{s_{NN}} = 200$ GeV. The 17.3-GeV data do not extend to high enough p_T to test quark-number scaling. We note, however, that the p_T where the v_2 values for mesons and baryons cross over each other (or, in the case of 17.3-GeV data, become similar) is approximately the same at all three center-of-mass energies. This indicates that identified particle v_2 at 17.3 GeV may also be consistent with quark-number scaling.

We also reported measurements of the higher harmonic term, v_4, for pions, kaons, protons, and $\Lambda + \overline{\Lambda}$. These measurements are also consistent with quark-number scaling laws arising from coalescence or recombination models [39]. This quark-number dependence may indicate that in ultrarelativistic heavy-ion collisions collective motion is established among quarks and gluons before hadrons are formed. This view is supported by the large v_2 values measured for multistrange baryons at $\sqrt{s_{NN}} = 62.4$ and 200 GeV [21]. Collisions involving lighter nuclei and larger, deformed nuclei (U+U) will provide another opportunity to study mass and quark number systematics for v_2. The possible approach to limiting values for v_2 (where the p_T and mass dependence at $p_T < 1$ GeV/c are consistent with hydrodynamic models) along with the evidence presented here that the relevant degrees of freedom in the early system may be subhadronic (e.g., *constituent quarks*) suggests that a strongly coupled matter with subhadronic degrees of freedom may be created in heavy-ion collisions at RHIC.

ACKNOWLEDGMENTS

We thank the RHIC Operations Group and RCF at BNL, and the NERSC Center at LBNL for their support. This work was supported in part by the Offices of NP and HEP within the U.S. DOE Office of Science; the U.S. NSF; the BMBF of Germany; CNRS/IN2P3, RA, RPL, and EMN of France; EPSRC of the United Kingdom; FAPESP of Brazil; the Russian Ministry of Science and Technology; the Ministry of Education and the NNSFC of China; IRP and GA of the Czech Republic, FOM of the Netherlands, DAE, DST, and CSIR of the Government of India; Swiss NSF; the Polish State Committee for Scientific Research; SRDA of Slovakia, and the Korea Science & Engineering Foundation.

[1] J.-Y. Ollitrault, Phys. Rev. D **46**, 229 (1992); H. Sorge, Phys. Rev. Lett. **82**, 2048 (1999).
[2] K. H. Ackermann *et al.* (STAR Collaboration), Phys. Rev. Lett. **86**, 402 (2001).
[3] B. B. Back *et al.* (PHOBOS Collaboration), Phys. Rev. Lett. **89**, 222301 (2002); K. Adcox *et al.* (PHENIX Collaboration), *ibid.* **89**, 212301 (2002).
[4] P. F. Kolb, J. Sollfrank, and U. W. Heinz, Phys. Rev. C **62**, 054909 (2000).
[5] M. Harrison, T. Ludlam, and S. Ozaki, Nucl. Instrum. Methods A **499**, 235 (2003).
[6] The reaction-plane angle is defined by the angle (relative to the laboratory frame) of the vector that connects the centers of the two colliding nuclei.
[7] S. Voloshin and Y. Zhang, Z. Phys. C **70**, 665 (1996).
[8] C. Adler *et al.* (STAR Collaboration), Phys. Rev. C **66**, 034904 (2002).
[9] C. Adler *et al.* (STAR Collaboration), Phys. Rev. Lett. **90**, 032301 (2003); J. Adams *et al.* (STAR Collaboration), *ibid.* **93**, 252301 (2004).
[10] P. Huovinen, P. F. Kolb, U. Heinz, P. V. Ruuskanen, and S. A. Voloshin, Phys. Lett. **B503**, 58 (2001).
[11] D. Teaney, J. Lauret, and E. V. Shuryak, Phys. Rev. Lett. **86**, 4783 (2001).
[12] C. Adler *et al.* (STAR Collaboration), Phys. Rev. Lett. **87**, 182301 (2001); **89**, 132301 (2002); S. S. Adler *et al.* (PHENIX Collaboration), *ibid.* **91**, 182301 (2003).
[13] J. Adams *et al.* (STAR Collaboration), Phys. Rev. C **72**, 014904 (2005).
[14] C. Alt *et al.* (NA49 Collaboration), Phys. Rev. C **68**, 034903 (2003).
[15] J. Adams *et al.* (STAR Collaboration), Phys. Rev. Lett. **92**, 052302 (2004); P. R. Sorensen, Ph.D. thesis, University of California-Los Angeles, 2003, arXiv:nucl-ex/0309003.
[16] S. A. Voloshin, Nucl. Phys. **A715**, 379 (2003); D. Molnar and S. A. Voloshin, Phys. Rev. Lett. **91**, 092301 (2003).
[17] R. C. Hwa and C. B. Yang, Phys. Rev. C **67**, 064902 (2003); V. Greco, C. M. Ko, and P. Levai, Phys. Rev. Lett. **90**, 202302 (2003); R. J. Fries, B. Muller, C. Nonaka, and S. A. Bass, *ibid.* **90**, 202303 (2003).

[18] S. S. Adler *et al*. (PHENIX Collaboration), Phys. Rev. Lett. **91**, 172301 (2003).
[19] S. F. Biagi *et al*., Nucl. Phys. **B186**, 1 (1981).
[20] J. Adams *et al*. (STAR Collaboration), Phys. Rev. Lett. **92**, 182301 (2004).
[21] J. Adams *et al*. (STAR Collaboration), Phys. Rev. Lett. **95**, 122301 (2005).
[22] K. H. Ackermann *et al*. (STAR Collaboration), Nucl. Instrum. Methods A **499**, 624 (2003).
[23] K. H. Ackermann *et al*. (STAR Collaboration), Nucl. Phys. **A661**, 681 (1999).
[24] J. Wu *et al*., Nucl. Instrum. Methods A **538**, 243 (2005).
[25] J. Adams *et al*. (STAR Collaboration), Phys. Rev. C **73**, 034906 (2006).
[26] M. Shao, O. Barannikova, X. Dong, Y. Fisyak, L. Ruan, P. Sorensen, and Z. Xu, Nucl. Instrum. Methods A **558**, 419 (2006).
[27] H. Bichsel, Nucl. Instrum. Methods A **562**, 154 (2006).
[28] A. M. Poskanzer and S. A. Voloshin, Phys. Rev. C **58**, 1671 (1998).
[29] M. Miller and R. Snellings, arXiv:nucl-ex/0312008.
[30] J. Adams *et al*. (STAR Collaboration), Phys. Rev. Lett. **92**, 112301 (2004).
[31] H. Sorge, H. Stoecker, and W. Greiner, Ann. Phys. **192**, 266 (1989); H. Sorge, Phys. Rev. C **52**, 3291 (1995).
[32] Y. Lu *et al*., J. Phys. G **32**, 1121 (2006).
[33] P. Sorensen (STAR Collaboration), J. Phys. G **30**, S217 (2004).
[34] A. Adare (PHENIX Collaboration), arXiv:nucl-ex/0608033.
[35] V. Greco and C. M. Ko, Phys. Rev. C **70**, 024901 (2004); X. Dong, S. Esumi, P. Sorensen, N. Xu, and Z. Xu, Phys. Lett. **B597**, 328 (2004).
[36] S. Manly *et al*. (PHOBOS Collaboration), Nucl. Phys. **A774**, 523 (2006).
[37] P. F. Kolb, Phys. Rev. C **68**, 031902 (2003).
[38] N. Borghini and J. Y. Ollitrault, Phys. Lett. **B642**, 227 (2006).
[39] L. W. Chen, C. M. Ko, and Z. W. Lin, Phys. Rev. C **69**, 031901 (2004); P. F. Kolb, L. W. Chen, V. Greco, and C. M. Ko, *ibid*. **69**, 051901 (2004); P. Sorensen, Acta Phys. Hung. A **24**, 221 (2005).
[40] J. Adams *et al*. (STAR Collaboration), Phys. Rev. Lett. **92**, 062301 (2004).
[41] We note that we are comparing $p + \overline{p}$ $v_2(p_T)$ for data sets with very different $\overline{p}/p$ yield ratios and in this article we have shown that the $\overline{\Lambda}$ v_2 is smaller than the Λ v_2.
[42] S. S. Adler *et al*. (PHENIX Collaboration), Phys. Rev. Lett. **94**, 232302 (2005).
[43] G. Agakichiev *et al*. (CERES/NA45 Collaboration), Phys. Rev. Lett. **92**, 032301 (2004).
[44] B. B. Back *et al*. (PHOBOS Collaboration), Phys. Rev. Lett. **94**, 122303 (2005).